Geometrical frustration of an argon monolayer adsorbed on the MgO (100) surface: An accurate periodic ab initio study

Geometrical frustration of an argon monolayer adsorbed on the MgO (100) surface: An accurate periodic *ab initio* study

Denis Usvyat,[1,*] Keyarash Sadeghian,[1] Lorenzo Maschio,[2] and Martin Schütz[1,†]

[1]*Institute for Physical and Theoretical Chemistry, Universität Regensburg, Universitätsstrasse 31, D-93040 Regensburg, Germany*

[2]*Dipartimento di Chimica and Centre of Excellence NIS (Nanostructured Interfaces and Surfaces), Università di Torino, via P. Giuria 5, I-10125 Torino, Italy*

(Received 2 April 2012; revised manuscript received 13 June 2012; published 9 July 2012)

We present an accurate first-principles method for calculating the energy of physisorption, based on a fully periodic local Møller-Plesset second order perturbation theory (LMP2) treatment. The LMP2 inter-surface-adsorbate interaction energy is scaled with a factor, obtained by comparing the method error of LMP2 versus coupled cluster singles doubles theory with perturbative triples at the basis set limit in small clusters mimicking the system under study. This method is applied to the investigation of geometrical frustration in argon monolayers adsorbed on the MgO (100) surface. It is found that several arrangements of the argon monolayer, i.e., 3×2, 4×2, optimal hexagonal, and $\zeta \times 2$ 1D noncommensurate have very similar adsorption energies, which agrees with the experimental observations. Moreover, this study provides further insight in to the Ar-MgO adsorption process and sheds light on a controversy among different experiments. The calculated adsorption energy of 2.3 kcal/mol is in a very good agreement with the experimental values, which range from 2.0 to 2.3 kcal/mol, and provides a new benchmark for this system.

DOI: 10.1103/PhysRevB.86.045412 PACS number(s): 68.35.Ja, 71.15.Nc, 31.15.A−, 31.10.+z

I. INTRODUCTION

Physisorption on crystalline surfaces is a fundamental process in nature and technology and therefore has been the subject of many experimental studies throughout many decades. Yet an accurate theoretical description of this phenomenon is inherently difficult, which is due to the fact that the energetics of physisorption are governed by a delicate balance between different attractive and repulsive components. Standard density functional theory (DFT), the dominating electronic structure method in solid state physics, does not describe van der Waals dispersion, which is one of the main driving forces for physisorption. Empirical dispersion correction schemes which blend the exchange-correlation functional with r^{-6}-dependent terms,[1–5] though quite practical,[6] are not a clean solution to this problem and provide only a qualitative level of description. One particular problem is the double counting of electron correlation in the intermediate range, where both the exchange-correlation functional as well as the damped dispersion correction contribute, which can compromise the form of the potential surface in an uncontrollable way (cf., e.g., Fig. 3 of Ref. 6).

State of the art orbital based correlation functionals like the random phase approximation (RPA)[7] include van der Waals dispersion in a rigorous way, but are computationally much more costly than standard DFT and not yet routinely used in calculations on periodic systems. Moreover, the influence of the choice of the underlying functional and the approximate treatment of exchange[8] still might remain an issue. For example, the direct RPA approach, being equivalent to ring-coupled cluster doubles without the exchange-type diagrams,[9] consequently contains exclusion principle violation diagrams, which are not canceled by the corresponding exchange terms.

Another route to the treatment of physisorption is the finite cluster approach, in particular, in combination with the incremental scheme.[10–12] Following this route, it is possible to employ high-level correlation methods available for molecular systems from the toolbox of quantum chemistry programs like coupled cluster singles doubles theory with perturbative triples [CCSD(T)] treatment. However, the proper modeling of a periodic structure by a finite cluster is difficult and the results may depend sensitively on the size and shape of the clusters, as well as on the embedding,[13] which have to be chosen and set up very carefully. This was observed to be critical even for molecular crystals,[14,15] and is assumed to be of even greater importance for ionic or covalent systems. Due to these issues the adequate clusters may become very large, then making high-level calculations prohibitively expensive.

A third possibility for theoretical treatment of physisorption is the use of fully periodic wave function based correlation methods. For systems with a large unit cell, the only avaliable method of this kind so far is Møller-Plesset perturbation theory of second order (MP2),[16–18] the simplest electron correlation theory. Within this method, in contrast to standard DFT, short- and long-range components of the adsorption energy are treated on the same footing, thus capturing the right physics of physisorption at least qualitatively. At the same time, the periodic nature of the systems involved is also properly taken into account. The deficiencies of the second-order method can be overcome to large extent by using a correction based on coupled cluster calculations on small clusters (*vide infra*).

For the present work, we used the periodic local MP2 (LMP2) method as implemented in the CRYSCOR program[17] to explore the physisorption of an argon monolayer on the magnesium oxide MgO (100) surface. In this method, the occupied and virtual spaces are spanned by localized orbitals, and for each pair of correlated electrons, the virtual space is truncated according to the spatial vicinity of the virtual orbitals to the corresponding occupied ones.[16,19,20] Furthermore, the pair approximation restricts the amount of electron pairs treated using a distance criterion. The unaccounted

correlation energy is recovered *a posteriori* via an C_6R^{-6}-type extrapolation.[17] For higher efficiency, the four-index electron repulsion integrals are evaluated by means of the density fitting technique[21,22] or multipole expansion.[16] This method has already been employed in a number of theoretical studies of periodic van der Waals systems.[23–26]

Adsorption of argon atoms on MgO surface is of fundamental interest as an example of a weakly bound frustrated monolayer, physisorbed on a surface of an oxide crystal. The MgO (100) surface (quadratic) and the Ar monolayer (hexagonal) are mutually *noncommensurate*. This results in geometrical frustration in the MgO (100)-Ar system, and the energetically most favorable coverage arrangement of Ar on MgO (100) is nontrivial to predict.

Adsorption of Ar on the MgO (100) surface has been studied experimentally some time ago by using volumetric measurements,[27,28] low-energy electron diffraction (LEED),[29,30] neutron scattering[28,31] and temperature programed desorption (TPD).[32] A certain controversy exists among the experimental studies concerning the arrangement of the argon monolayer on MgO. Initial experiments[29] conducted at temperatures $49 < T < 66$ K report the 3×2 (see Sec. II C for the nomenclature) and the hexagonal packing of the monolayer. In a refined lower-temperature ($25 < T < 36$ K) experiment, the 3×2-structure is also observed, yet at high coverage it is superseded by the 4×2 geometry, while the hexagonal arrangement is observed only together with the onset of the second argon layer condensation.[30] In a later neutron diffraction study at 10 K, on highly homogeneous MgO powder surfaces the hexagonal structure has been again observed at high coverage, but before the second layer condensation.[28] Furthermore, at temperatures 35–40 K a "one-dimensional" melting from the 3×2 structures, resulting in a 1D noncommensurate $\zeta \times 2$ arrangement has been observed.[28,31] The reported experimental adsorption energy[27,29–31] lies in the range of 2.0–2.3 kcal/mol per Ar atom (with a relatively large error bar of 0.3 kcal/mol or more). Calculations based on empirical model potentials have been carried out,[30] which favor the 3×2 and 4×2 arrangements. On the basis of these calculations, the hexagonal structure has been dismissed as energetically noncompetitive.

The smallness of the adsorbate molecules (which are just atoms in this case) and rich experimental data on the one hand, but a number of remaining open questions and computational and methodological challenges on the other hand, make Ar-MgO an ideal first-application system for the high-quality *ab initio* technique proposed in this contribution. In the present work, we study the geometrical frustration of the argon monolayer on the MgO (100) surface *ab initio* and fully periodic at the MP2 level, with corrections from CCSD(T) finite cluster calculations. As will be shown below, very good agreement with experimental adsorption energies is achieved. Moreover, the analysis of the results of the calculations allows for further insights into the mechanism of the adsorption process, which can help in resolving the controversy among the experimental observations. Apart from presenting the results of this particular application to argon adsorbed on MgO, the present work also serves as a general recipe on how to calculate accurate adsorption energies by employing the periodic local MP2 method implemented in the CRYSCOR program in conjunction with higher order corrections from finite cluster calculations.

II. METHOD

A. The energy of adsorption

The energy of adsorption of the argon monolayer on the MgO substrate at zero temperature $\Delta E_{T=0}$ is defined in the Born-Oppenheimer approximation as a sum of two contributions: (i) the electronic energy ΔE_e and (ii) the zero-point vibrational energy of the atoms ΔE_{ZPE}. The major component is obviously the electronic binding energy, which therefore has to be computed with high accuracy. We calculate this energy as the sum of the *vertical* monolayer-slab (MS) interaction energy per argon atom,

$$\Delta E_{\perp} = (1/N_{\mathrm{Ar}})(E_{\mathrm{MS}} - E_{\mathrm{M}} - E_{\mathrm{S}}), \tag{1}$$

and the lateral argon-argon interaction energy per argon atom,

$$\Delta E_{\parallel} = (1/N_{\mathrm{Ar}})E_{\mathrm{M}} - E_{\mathrm{Ar}}, \tag{2}$$

where E_{Ar} is the energy of an isolated argon atom and N_{Ar} is the number of argon atoms in the unit cell. $E_{\perp}$ and $E_{\parallel}$ are computed by utilizing the periodic local MP2 method implemented in the CRYSCOR program.[16,17,33] The periodic Hartree-Fock (HF) reference and the localized orbitals used by CRYSCOR are generated by the CRYSTAL program.[34–36] In this work, a relatively rich basis set of triple-ζ quality for Mg [$5s4p2d1f$] and augmented-triple-ζ quality for oxygen [$5s4p3d2f$] and Ar ([$4s4p3d2f$] with effective core potential), are employed (see Appendix A for a detailed specification). We will use in the following the acronym AVTZ' to denote this basis set. In order to achieve high accuracy, the MP2 energies are further corrected according to a scheme based on CCSD(T) energies at the basis set limit, which are obtained from finite cluster calculations. This correction scheme is explained in details in Sec. II B.

In order to eliminate the basis-set superposition error (BSSE), $E_{\perp}$ and $E_{\parallel}$ are counterpoise corrected[37] by including the ghost argon-monolayer and ghost MgO slab for E_S and E_M, respectively, in Eq. (1), and surrounding the argon atom by 18 nearest-neighbor ghost atoms for E_{Ar} in Eq. (2).

Frozen core (core electrons are not correlated) LMP2 calculations are carried out for several competing geometrical arrangements, which are discussed in detail in Sec. II C. The Ar monolayer might be not entirely planar due to the corrugation of the substrate potential. The Ar-slab distances for different adsorption sites are obtained as the minima of the corresponding individual Ar-MgO potential curves, as explained in the same section.

The core contribution (the difference between the core-correlated and frozen core interaction energies) to the adsorption energy is relatively small (about 8% of the frozen core interaction energy), but essential at the scale of the energy differences under study. Since calculations involving core correlation, which also require enlarged basis sets (from the cc-pwCVXZ family[38]), are rather expensive, these contributions have been calculated using supercells of smaller size and under the assumption of a sinelike form of the corrugation potential (see Sec. II D for details).

Surface relaxation effects are calculated at the DFT-D2 (PBE functional[39]) level[40,41] as the difference between the (BSSE uncorrected) electronic adsorption energies of the individual Ar-MgO arrangements, (i) fully optimized, and (ii) optimized with the Mg-O distance constrained to the experimental value of of 2.105 Å. In these geometry optimizations, carried out with the CRYSTAL program,[42] the 2D unit cell parameters are kept fixed. The D2 parameters for the Mg and O atoms were taken from Ref. 6, those for argon, as well as the s_6 parameter for PBE, from the original DFT-D2 paper.[40] The experimental Mg-O distance is used for both the MgO slab and the finite cluster (cf. Sec. II B) in all periodic LMP2 and coupled cluster calculations.

Finally, ΔE_{ZPE} is calculated as the difference between the DFT-D2 zero-point energies of the slab with and without the adsorbate. The corresponding harmonic vibrational frequencies and normal modes were computed with the CRYSTAL program.[43] Additionally, the ΔE_{ZPE} contribution related to those modes of the Ar atoms vibrating perpendicular to the surface, were also calculated beyond the harmonic approximation in the very accurate corrected LMP2 Ar-MgO 1D potentials, employing the ANHARM program.[44] For these calculations, the mass of the MgO crystal is assumed to be infinite, and the dispersion of the vibrational bands corresponding to the perpendicular modes is neglected.

B. Finite cluster calculations and correction scheme for periodic LMP2

The geometrical frustration of the argon monolayer on MgO (100) is caused by the competition between (i) the interactions within the monolayer itself favoring a hexagonal arrangement and (ii) the interaction between the individual argons with the MgO (100) surface favoring a quadratic arrangement (each argon on top of every second Mg atom). This competition leads to multiple adsorption arrangements close in energy. Since both competing interactions are of similar magnitude (*vide infra*) an accurate and balanced description is required. Otherwise, if, due to deficiencies in the theoretical treatment, one of the competing interactions is artificially accentuated relative to the other, wrong predictions for the adsorption arrangements would be obtained. The most important error sources are (i) the MP2 method itself, (ii) the incomplete basis set, and (iii) the local approximation. MP2 is known to noticeably underestimate van der Waals dispersion for systems with low polarizability, while overestimating it for systems with high polarizability. Furthermore, the smallness of the interaction energies studied here requires large basis sets. In this work, we employ already a relatively rich basis set for the periodic LMP2 calculations. However, the use of molecular basis set hierarchies and basis set extrapolation techniques are not possible in the periodic context due to quasilinear dependency problems.[45] Finally, the truncation of the virtual space to pair domains in the local approximation inflicts a further, though much smaller *domain error*. These errors can be avoided to large extent by the following correction scheme, which follows the same train of thought as the hierarchical approaches proposed recently.[6,46]

Local correlation methods, as discussed in detail before,[17,47] offer the possibility to partition the correlation part of intermolecular interactions. Of prime concern here is a partitioning of it into an intra- and an interpart, i.e., into a part summing up pair energies with the two localized occupied orbitals (Wannier functions) residing on the same subsystem (MgO slab or Ar monolayer), and a part summing up pair energies with the two localized occupied orbitals residing on *different* subsystems. In order to repair the deficiency of the MP2 method with respect to over- or underestimation of van der Waals dispersion, it can be sufficient to scale the inter part according to a higher-order method. Also the basis set truncation effects and the domain error can be folded into the scaling of the inter part. The scaling factor is obtained from finite cluster calculations by comparing LMP2 potential energy curves (employing same basis set and domains as the periodic LMP2 calculation) to basis set extrapolated CCSD(T) potential energy curves. We note in passing, that for local CCSD(T) calculations a simple incremental correction at the MP2 level fixes the basis set truncation as well as the domain error, yielding CCSD(T) results close to the basis set limit.[48,49]

The finite clusters utilized to mimic the intralayer argon-argon, and the interlayer-slab argon-MgO interactions are the equilateral argon trimer, and the Ar-$Na_2Mg_3O_4$ dimer (depicted in Appendix B), respectively. In the latter, the MgO-part is a quadratic planar cut from the periodic slab with two sodium atoms (yet with Mg basis set) substituting the border Mg atoms to preserve charge neutrality. The Ar atom is placed on top of the central Mg atom at various distances. Ar_3 as well as Ar-$Na_2Mg_3O_4$ are still small enough to allow for canonical CCSD(T) calculations in good basis sets. The LMP2 calculations are performed in the AVTZ' basis (same basis as employed in periodic calculations), while the CCSD(T) correlation energies are extrapolated to the basis set limit according to the standard inverted cubic formula[50] based on calculations in the aug-cc-pVTZ and aug-cc-pVQZ basis sets.[51] The HF part of the interaction energy is not extrapolated, but calculated directly in the aug-cc-pVQZ basis. Further details specifying the finite cluster calculations are given in Appendix B.

MP2 is known to *overestimate* the interaction energies of Ar clusters at the basis set limit,[14,52] and to *underestimate* the interaction energies of systems involving MgO.[6,25,26,53] Figure 1 shows the LMP2 and CCSD(T) potential energy curves for the equilateral Ar_3. Evidently, over the whole

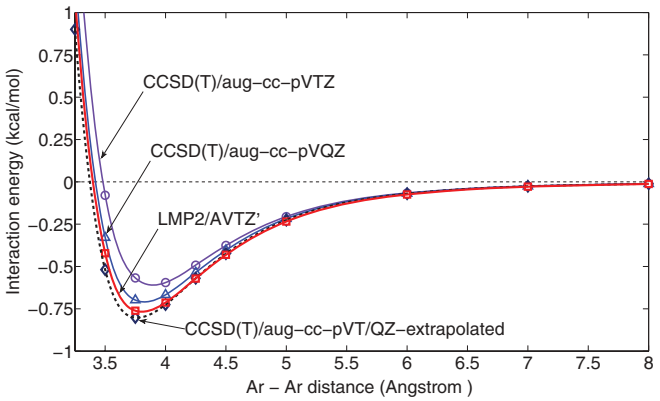

FIG. 1. (Color online) CCSD(T) and LMP2 potential curves for the equilateral argon trimer.

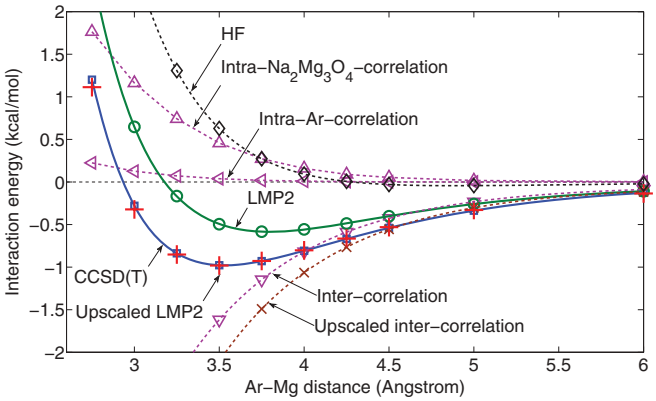

FIG. 2. (Color online) HF, LMP2, CCSD(T), and corrected LMP2 potential curves for the argon - planar $Na_2Mg_3O_4$ dimer in the perpendicular orientation. The intra- and intercomponents of the LMP2 and corrected LMP2 curves are also shown.

range of Ar-Ar distances LMP2/AVTZ' virtually reproduces the CCSD(T) result at the extrapolated basis set limit. This is due to a fortuitous error compensation between the basis set deficiency of the AVTZ' basis and the tendency of MP2 to overestimate the Ar-Ar interaction. Note that at the MP2 level three-body dispersion (Axilrod-Teller) contributions are absent (they appear first at the MP3 level), while other more important nonadditive contributions are captured. In any case, for the description of the intralayer argon-argon interactions the LMP2 method in the AVTZ' basis performs very well and no further correction is applied.

The situation, however, is different for the Ar-MgO interaction, as Fig. 2 clearly shows. This interaction is significantly underestimated by MP2, as already observed before for other gases (helium or methane), adsorbed on MgO.[6,25,26] Here, the errors of method and basis set incompleteness are of the same sign. Consequently, the LMP2/AVTZ' potential energy curve lies significantly above the curve of CCSD(T) at the basis set limit. A pure (uncorrected) LMP2/AVTZ' description of the Ar monolayer adsorbed on MgO thus would be biased towards a hexagonal arrangements, and a fair prediction of geometrical frustration spoiled.

The deficiencies of the MP2 method manifest primarily in the intermolecular component of the interaction energy, which comprises dispersion, exchange-dispersion, and dispersion-induction types of interaction.[54,55] The intrapart, i.e., the reduction of the correlation energy of the electrons of the Ar atom due to exchange compression caused by the presence of the electron density of the $Na_2Mg_3O_4$ cluster and *vice versa* is, on the other hand, rather well described. Indeed, as is evident from Fig. 2, the CCSD(T) reference curve is faithfully reproduced over the whole range of Ar-MgO distances by LMP2/AVTZ' after scaling its intermolecular pair energies by a factor of 1.3. This scaling factor thus is utilized in all subsequent periodic LMP2/AVTZ' calculations, i.e., all pair energies corresponding to one Wannier function being localized within the Ar monolayer, and the other within the MgO slab, are scaled by 1.3. The LMP2/AVTZ' results, obtained after such a scaling of the intermolecular (inter slab-adsorbate) energies, are referred to as *corrected LMP2*.

Within this procedure the cluster calculations are utilized not to calculate an incremental energy correction to the periodic result (for which the clusters considered are indeed much too small), but rather a correcting factor for the LMP2 method itself for this particular system. In closely related systems, where the physics behind the interaction is similar, the MP2 method can be expected to behave also very similarly regarding the accuracy. The scaling factor for the LMP2 intermonomer correlation contribution, obtained from the cluster calculations, is therefore expected to be accurate for the Ar monolayer adsorbed on a MgO surface. A scheme as the one described here, employing parameters specific for the type of the system, is clearly superior in accuracy relative to the commonly used more general scaling techniques like spin component scaled MP2,[56] double-hybrid DFT,[57] DFT-D2,[40] or MP2-D,[58] where universal parameters, fitted for a large set of small systems, are employed to determine the parameters for good.

C. Models for commensurate argon monolayers adsorbed on MgO (100)

Before discussing the different energetically competitive geometrical arrangements of the argon monolayer adsorbed on top of the MgO (100) surface we consider here a model for a single argon atom adsorbed on MgO (100). Since argon atoms do not carry any electrostatic moments, no electrostatic and only weak inductive components contribute to the adsorption energy. So the main components are long-range attractive van der Waals dispersion versus short-range exchange repulsion.

Figure 3 displays the CCSD(T)-corrected LMP2/AVTZ' potential energy curves of Ar adsorbed on top of the Mg and O sites, respectively. For these (periodic) calculations, a commensurate [with respect to MgO (100)] square arrangement of the Ar monolayer was employed, with its unit cell matching the doubled cell of the MgO surface. According to the nomenclature introduced below this arrangement is denoted by 2×2. The Ar-Ar interaction in 2×2 is rather small (*vide infra*). Apart from the total Ar-MgO interaction energies also the curves of its individual components, i.e., the Hartree-Fock part (almost exclusively exchange repulsion), and the

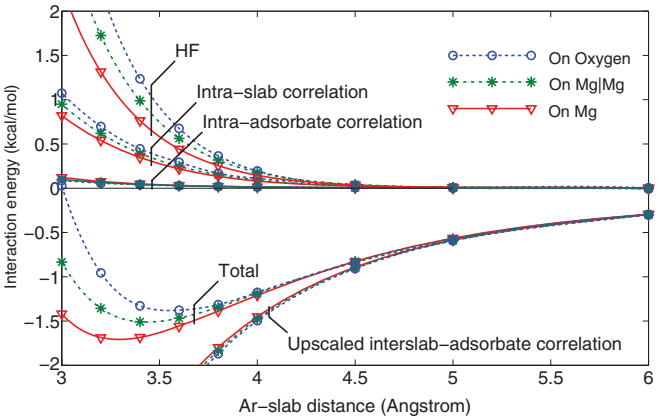

FIG. 3. (Color online) Corrected LMP2 Ar-MgO potential curves and its components, calculated in the 2×2 arrangement for 3 adsorption positions: on top of Mg atoms (red, triangles, solid), on top of oxygen atoms (blue, circles, dashed) and on top of Mg-Mg midpoint (green, starts, dash-dotted).

intralayer, intraslab, and interlayer-slab correlation energies (the latter almost exclusively van der Waals dispersion) are shown in Fig. 3. Evidently, the intralayer, and intraslab correlation energies, as well as the interlayer-slab van der Waals dispersion, are relatively insensitive with respect to the adsorption site. This fact further justifies our correction scheme, based solely on calculations on the Ar-$Na_2Mg_3O_4$ dimer, where Ar sits atop of the Mg site.

The onset of the exponential exchange wall, on the other hand, which crucially depends on the shape of the one-particle density function at the surface, is site specific. Due to the ionicity of the MgO crystal and its surface, with the electron density concentrating around the O atoms, the Mg site is energetically most favored. Its late onset of the exchange repulsion wall allows for the closest approach of an Ar atom towards the surface, hence for the largest van der Waals attraction. For analogous reasons, the O site is the least favorable for Ar adsorption.

Based on this knowledge, qualitative predictions about possible candidates for competing arrangements are already possible. The noncommensurate hexagonal structure with the shortest Ar-Ar distance of 3.8 Å, which is the preferred geometry of the isolated monolayer (cf. Sec. III B), is the limiting case in terms of maximal strength of the lateral interaction and, at the same time, minimal strength of the Ar-MgO binding. The latter suffers from loss of registry with the surface, occupying thus nonoptimal adsorption sites, including the least attractive on-oxygen position as well as any other site. The frustrated quadratic 2×2 argon monolayer [cf. Fig. 4(a)] is the other limiting case. Here, any Ar atom always sits on top of the preferred Mg site, yet the Ar-Ar distance of 4.21 Å is much longer than in the optimal hexagonal packing, leading to very weak Ar-Ar interactions. The intermediate frustrated rectangular arrangements 3×2 [see Fig. 4(b)] and 4×2 [see Fig. 4(c)] feature close to optimal Ar-Ar distances (yet not in a hexagonal packing), and, at the same time, none of the on-oxygen, or close to on-oxygen positions are occupied. The cubic 3×3 [see Fig. 4(d)] structure is quite close to a hexagonal structure, yet with a somewhat longer Ar-Ar distance. Obviously, the real noncommensurate hexagonal structure is not periodic and thus cannot be studied as is within a periodic quantum chemical treatment. In Ref. 30, it was mimicked by a very large commensurate 9×13 supercell, which is presently beyond reach for our *ab initio* treatment. We have found, that an alternative and substantially smaller commensurate structure, shown in Fig. 4(e), is also very close to the optimal hexagonal arrangement. This supercell, denoted as hexlike, comprises 134 atoms (within the 3-layer MgO-slab model) and is thus treatable at the periodic LMP2 level.

In these five competing arrangements the Ar atoms occupy 11 symmetry unique sites on the MgO (100) surface. Obviously, the optimal Ar-MgO distance depends on the individual site. Since a full optimization of the individual adsorption arrangements on the counterpoise and CCSD(T)-corrected LMP2 potential energy surface is unfeasible, the individual site specific optimal distances are calculated for the 2×2 square argon monolayer, where each Ar is adsorbed atop of an equivalent MgO site. The 2×2 square argon monolayer is shifted against MgO such that the Ar atom is centered at the required site position. For each of the eleven site positions,

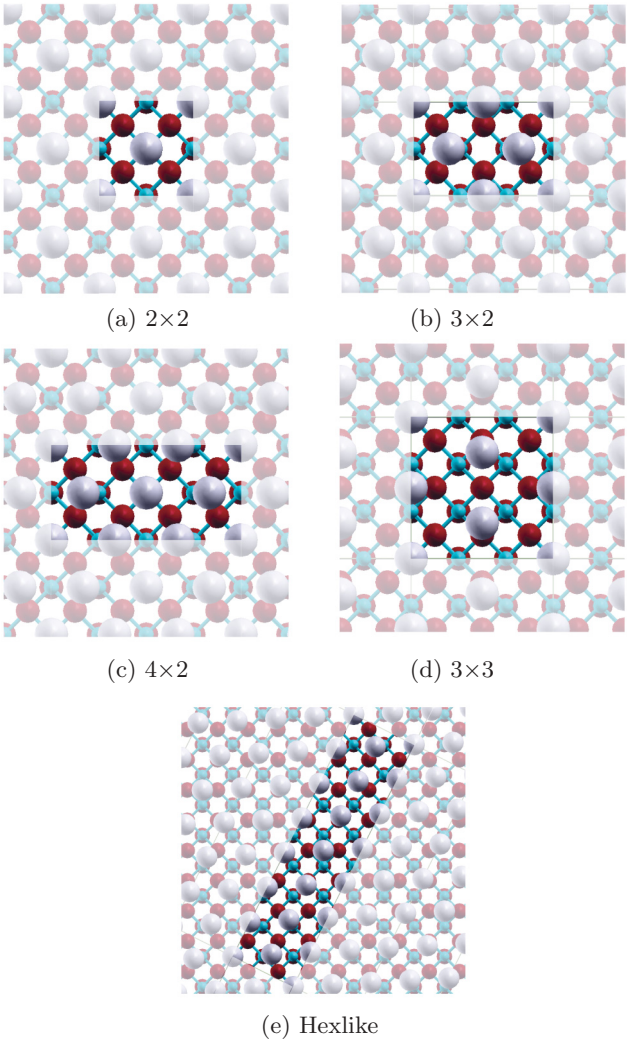

FIG. 4. (Color online) The competing arrangements of argon monolayer on MgO surface, studied in the present work. Small blue spheres correspond to the Mg atoms, intermediate-sized red spheres to the oxygen atoms, and large grey spheres to the argons. The crystallographic unit cells are brightened. The detailed specification is given in Appendix C.

the Ar-MgO distance was varied and a potential energy curve computed (frozen core approximation, *vide supra*). The data of all these eleven points plus the on-oxygen position are provided in Appendix C. The minima of the curves then are determined via cubic splines, yielding the respective minimum energies and optimal distances. The latter are then further used as the optimal Ar-MgO site-specific distances for the different adsorption positions in the actual supercell LMP2 calculations.

The shortest and longest distances of 3.29 and 3.55 Å, respectively, obviously correspond to the on-Mg and on-O sites (cf. Fig. 3); the other site-specific optimal distances all lie within this interval, for example, for the Mg-Mg midpoint position (Mg|Mg), it amounts to 3.44 Å. We also note that the corresponding values reported in Ref. 30 (which were calculated by using a model potential) are noticeably shorter, i.e., 2.92 Å for on-Mg and 3.07 Å for the Mg|Mg positions, respectively.

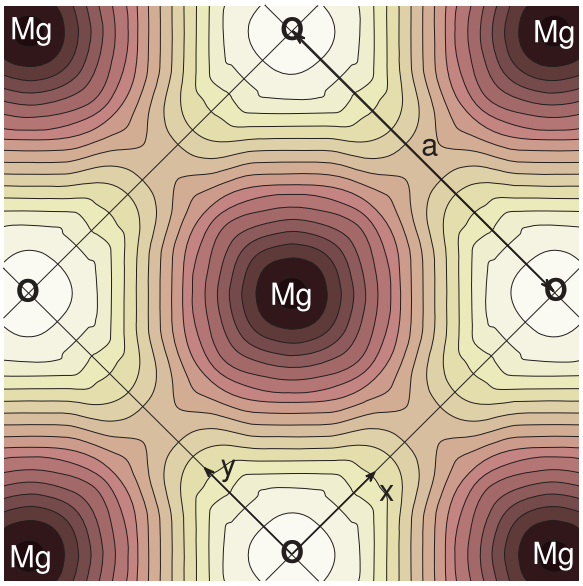

FIG. 5. (Color online) The MgO (100)-surface corrugation potential for the argon atoms at the equilibrium Ar-MgO distance. The 2D surface has been fitted via a cubic interpolation to the energies for 12 symmetry unique adsorption sites, calculated within the 2×2 supercell. The maximal and minimal energy values are -1.381 kcal/mol (on-O adsorption) and -1.709 kcal/mol (on-Mg adsorption). The contour isoline step is 0.02 kcal/mol.

D. Models for noncommensurate argon monolayers adsorbed on MgO (100)

The calculated potential energies of the 12 calculated adsorption sites (11 sites, corresponding to the studied structures, see Sec. II C, plus the on-oxygen site) can be utilized to construct by interpolation the relaxed (with respect to Ar-MgO distance) potential energy surface $\Delta E_\perp(x,y)$, where x and y are the coordinates specifying the site position of the Ar on the MgO lattice.

Figure 5 displays the contour plot of this surface as generated by a cubic fit. This "corrugation potential" yields $\Delta E_\perp$ for any site position. Its shape suggests that it can be represented by the simple trigonometric model potential:

$$\Delta E_\perp(x,y) = A + B[\cos(2\pi x/a) + \cos(2\pi y/a)] + C\cos(2\pi x/a)\cos(2\pi y/a), \quad (3)$$

where $a = 2.9769$ Å is the lattice constant of the MgO surface, x and y are the coordinates along the mutually perpendicular O-O directions with the origin being placed at the on-O position. The parameters A, B, and C are determined such that the three most important points on this potential surface, i.e., $E_\perp^{\mathrm{Mg}}$ (the minimum), $E_\perp^{\mathrm{O}}$ (the maximum) and $E_\perp^{\mathrm{Mg|Mg}}$ (the saddle point) are reproduced exactly, which yields

$$\begin{aligned} A &= 1/2[\Delta E_\perp^{\mathrm{Mg|Mg}} + 1/2(E_\perp^{\mathrm{Mg}} + E_\perp^{\mathrm{O}})], \\ B &= 1/4[\Delta E_\perp^{\mathrm{O}} - E_\perp^{\mathrm{Mg}}], \\ C &= 1/2[-\Delta E_\perp^{\mathrm{Mg|Mg}} + 1/2(E_\perp^{\mathrm{Mg}} + E_\perp^{\mathrm{O}})]. \end{aligned} \quad (4)$$

Using this corrugation potential it is easily possible to assess $\Delta E_\perp$ for noncommensurate adsorption arrangements. Since in a 2D noncommensurate monolayer (like the exact hexagonal packing), any of the adsorption position is equally populated, its $\Delta E_\perp$ is obtained through a 2D integration over the potential surface. From the fitted potential of Fig. 5, and from Eq. (3) one then gets the values of -1.520 and -1.528 kcal/mol, respectively, which are very close indeed.

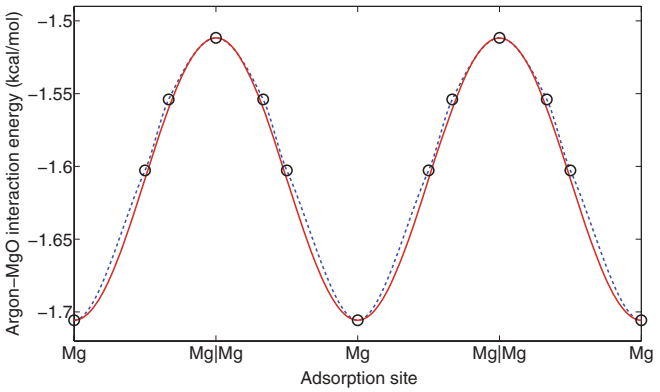

FIG. 6. (Color online) The MgO (100)-surface corrugation potential curve along the Mg-(Mg|Mg)-Mg direction as from the 2D 12-point cubic fit, Fig. 5 (blue dashed line) or from Eq. (3) (red solid line). The energies of explicitly calculated points within this direction are also shown (circles).

Of interest in the present context are also the 1D noncommensurate $\zeta \times 2$ arrangements (ζ stands for an irrational number).[28,31] Here, the Ar atoms populate sites along the Mg-Mg direction; the on-O site is never occupied. These arrangements correspond, e.g., to intermediate structures between 2×2 and 3×2 (cf. Fig. 4), etc. The curves of the fitted (Fig. 5) and model [Eq. (3)] potential, and the explicitly calculated points along this direction are shown in Fig. 6. For $\zeta \times 2$ noncommensurate arrangements the $\Delta E_\perp^{\zeta\times 2}$ can be calculated by integrating the 1D potential curve of Fig. 6, which in the case of the model potential (3) is equivalent to the arithmetic mean of $\Delta E_\perp^{\mathrm{Mg|Mg}}$ and $\Delta E_\perp^{\mathrm{Mg}}$, yielding 1.610 kcal/mol. Integrating the cubic-fit curve instead yields -1.604 kcal/mol, which again is very close to the previous value. We conclude that the model potential (3) is very accurate despite its simplicity (just three points are needed to specify it). It thus will be used further in the subsequent section.

III. RESULTS AND DISCUSSION

A. Vertical Ar-MgO interactions $\Delta E_\perp$

Table I compiles the monolayer-slab interaction energies $\Delta E_\perp$ per argon atom, corresponding to the 2×2 corrected-LMP2 minima, of the five competing arrangements studied in this work. Clearly, $\Delta E_\perp$ calculated with the CCSD(T)-corrected LMP2 scheme is substantially more negative (by 0.6–0.7 kcal/mol in absolute value) than $\Delta E_\perp$ as provided by the pure LMP2 approach. Employing the true LMP2 minima, rather than the corrected-LMP2 ones, the magnitude of the pure LMP2 interaction energies increase slightly in absolute value, but not by more than 0.08 kcal/mol. Thus the CCSD(T) correction clearly is mandatory in this case to arrive at sufficiently accurate results.

Rather than performing the full supercell calculation, a cheap but quite accurate estimate for $\Delta E_\perp$ is obtained by

TABLE I. The corrected LMP2 (and pure LMP2 in parenthesis) Ar-MgO slab interaction energy $\Delta E_\perp$ per argon atom for different arrangements of the argon monolayer. The correcting factor for the LMP2 inter-components of 1.3, as obtained from the calculations on a Ar-$Na_2Mg_2O_4$ dimer (see sect. II B), has been used. The argon atoms are placed according to the minima of the individual Ar-MgO corrected LMP2 potential curves, evaluated with the 2×2 supercell (cf. Sec. II C). The commensurate phase interaction energies, calculated both within the full supercell approach, and by adding up the corresponding energies from the corrected LMP2 minima of the individual Ar-MgO potential curves, are given. The noncommensurate phase energies are those obtained by integrating the potential (3). All values are given in kcal/mol.

Structure	$\Delta E_\perp$ per argon atom	
	Commensurate structures	
	Full supercell	Sum of individual 2×2 $\Delta E_\perp$
3×3	$-1.509(-0.877)$	$-1.527(-0.888)$
2×2	$-1.709(-0.974)$	$-1.709(-0.974)$
3×2	$-1.601(-0.931)$	$-1.607(-0.928)$
Hexlike	$-1.506(-0.881)$	$-1.520(-0.887)$
4×2	$-1.611(-0.944)$	$-1.606(-0.929)$
	Noncommensurate structures	
	Integrated from Eq. (3)	
2D noncommensurate	$-1.528(-0.887)$	
$\zeta \times 2$	$-1.610(-0.928)$	

appropriate summation of the individual Ar-MgO interaction energies of the respective minima, which are calculated for each Ar in the supercell *separately* within the 2×2 model (cf. Sec. II C). For this approach, the change in the three-body (and higher) terms involving two (or more) Ar atoms and the MgO slab in the actual structure relative to 2×2 are neglected. Apparently, this deficiency is not troublesome for the present system; as is evident from Table I the deviations from the full supercell calculation are at most 0.02 kcal/mol. The changes in the HF and correlation three-body terms are small by themselves, and, moreover, appear with opposite sign, such that their sum is further reduced. For example, for the 4×2 arrangement the difference in the HF (repulsive) contributions between the full supercell and the approximated (pair-potential) calculations is -0.032 kcal/mol, while the corresponding difference in the correlation parts amounts to 0.025 kcal/mol. As already mentioned, the three-body Axilrod-Teller dispersion is not captured by the MP2 method, yet some part of it, e.g., the O-O-Ar term is effectively included by the CCSD(T) correction (evaluated for the on-Mg adsorption site in the finite cluster). Since the actual three-body dispersion contribution is expected to be small, and dispersion *per se* is isotropic (cf. Sec. II C) its site dependence is assumed to be very small.

The $\Delta E_\perp$ values of the 2D and $\zeta \times 2$ noncommensurate arrangements in Table I are calculated by integration of Eq. (3), as discussed in Sec. II D. Strikingly, when comparing these with the $\Delta E_\perp$ values of the commensurate arrangements the $\Delta E_\perp$ values divide in three groups. The first group comprises the hexlike, the 3×3 (also close to hexagonal, but with larger Ar-Ar distance), and the 2D noncommensurate arrangements all have a very similar $\Delta E_\perp$ of -1.51–-1.53 kcal/mol. The members of the second group are the 3×2, 4×2, and the 1D noncommensurate $\zeta \times 2$ arrangements with a $\Delta E_\perp$ of -1.60–-1.61 kcal/mol. The third group finally just includes 2×2 with a $\Delta E_\perp$ of -1.71 kcal/mol, where only the most preferable on-Mg site is populated. Just a slight elongation or compression of the 2×2 monolayer unit cell relative to that of the slab along the Mg-Mg coordinate should lead to $\zeta \times 2$ with a weaker MgO-Ar attraction (that of the second group). Similarly, just a slight perturbation of the monolayer unit cell corresponding to any structure of the second group relative to the slab unit cell along the direction perpendicular to the Mg-Mg coordinate immediately leads to the 2D noncommensurate arrangement with a further weakened MgO-Ar attraction.

The $\Delta E_\perp$ values in Table I are all based on frozen core calculations. Appreciating the accuracy of the pair-, and of the corrugation model potential defined in Eq. (3) the (computationally considerably mode demanding) periodic LMP2 calculations including core correlation were just performed for the 2×2 supercell with the Ar placed on the Mg, oxygen, and Mg|Mg sites at their individual optimal Ar-MgO distances. The core correlation contribution to $\Delta E_\perp$ for these three geometries then is computed by subtracting from the resulting $\Delta E_\perp$ the corresponding $\Delta E_\perp$ in the frozen core approximation. The core correlation contributions to $\Delta E_\perp$ (which mainly describe van der Waals dispersion between Mg core electrons an Ar) turn out to be not very site specific. One obtains -0.168, -0.141, and -0.138 kcal/mol, for the Mg, Mg|Mg and oxygen positions, respectively. To calculate the core correlation contribution at an arbitrary site the corrugation model potential of Eq. (3) again is utilized, which is completely specified by these three numbers.

B. Lateral Ar-Ar interactions $\Delta E_\parallel$

The second—lateral—contribution to the adsorption energy, $\Delta E_\parallel$, is smaller than $\Delta E_\perp$, but still important at the scale of the total interaction energy. Moreover, its size is very sensitive to the density of the Ar monolayer, and with that to the particular arrangement of the Ar atoms. Therefore, $\Delta E_\parallel$ can be decisive for the relative stability of the five different arrangements shown in Fig. 4.

Figure 7 displays the individual $\Delta E_\parallel$ of these five arrangements (marked by crosses) as a function of the density, or surface concentration, σ (number of Ar atoms per MgO surface unit cell). The actual nonplanarity of the monolayer (due to the vertical Ar-MgO interaction) is taken into account for four points (the 2×2 monolayer is planar), even though just the monolayer alone is considered here. The $\Delta E_\parallel$ curves for (i) arbitrary rectangular $\zeta \times 2$ (and $n \times 2$) and (ii) hexagonal monolayers with varying Ar-Ar distances are also plotted. Evidently, the $\Delta E_\parallel$ is quite insensitive to the small out-of-plane displacements of the Ar atoms caused by the vertical $\Delta E_\perp$, the only visible deviation from the corresponding curve appears for 4×2, which already is at the onset of the repulsive side of the potential and thus even slightly benefits from nonplanarity of the monolayer.

It can also be seen that the hexlike structure indeed is very close to the (noncommensurate) optimal hexagonal Ar monolayer, both in terms of σ and $\Delta E_\parallel$. The calculated Ar-Ar

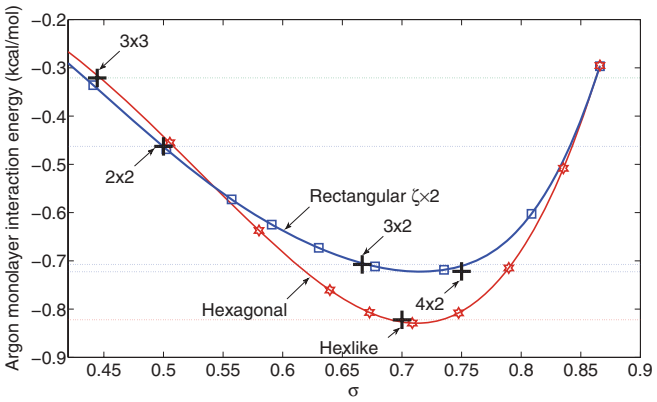

FIG. 7. (Color online) The formation energy of the planar argon monolayer per one argon atom $E_{\|}$ as a function of the surface concentration σ, i.e., the number of Ar atoms per MgO surface unit cell (unity concentration corresponds to an arrangement with the amount of Ar atoms equal to that of surface Mg or O atoms). Two types of arrangements are considered: the continuous rectangular $\zeta \times 2$ arrangement (and $n \times 2$ with the 2×2, 3×2, and 4×2 geometries as particular cases): blue squares; and a regular hexagonal monolayer with different inter-argon distances: red stars. The symbols represent the explicitly calculated points, the values in between are spline interpolated. The crosses correspond to the energies of the five commensurate argon monolayer arrangements studied in the paper, calculated with the actual off-planarity of the argon atoms in the monolayers (cf. Sec. II C) taken into account.

distance of the latter is 3.8 Å, which is in quite good agreement with the experimental distance of 3.76 Å observed in the LEED experiments of Ref. 30. Note that the hexagonal Ar monolayer in these experiments is only observed after the onset of the second monolayer condensation, which due to the additional Ar-Ar interactions may lead to shortening of the Ar-Ar distances in the first layer (in the argon crystal e.g the optimal Ar-Ar distance is 3.70 Å).

The optimal hexagonal structure is about 0.1 kcal/mol more stable than the $\zeta \times 2$ one, but the effect of the stabilization of the hexagonal structure with respect to the rectangular one is restricted to a relatively short range of concentrations ($0.6 < \sigma < 0.8$). The densities of the 3×2 and 4×2 arrangements are located at opposite sides of the minimum of the $\zeta \times 2$ potential curve and the corresponding energies $\Delta E_{\|}$ virtually coincide with each other. Moreover, due to a shallowness of the potential near the minimum, these energies are very close to the minimal energy itself. The 2×2 and, especially, 3×3 structures, on the other hand, are much more sparse than the other three, which translates to substantially weaker lateral binding energies for these two arrangements.

C. Vibrational zero-point energies

Automatic optimization of the geometry and calculation of vibrational frequencies at the LMP2 level is not possible presently. Therefore the ZPEs as well as surface relaxation effects have been evaluated at the DFT-D2 level. Note that the CRYSTAL program presently is limited to calculations of Γ-point vibrations. For each of the five studied Ar-MgO structures, the vibrational frequencies have been computed at the DFT-D2-optimized geometries. In all the structures, apart from 2×2, the unit cell contains several argon atoms. Therefore the Γ-point vibrations of these lattices formally comprise vibrations which correspond to several k points of the monoatomic cell case. For example, the vibrations related to antiphase displacements of the argon atoms are also included. For the 2×2 structure, which contains just one argon atom per primitive unit cell, the frequency calculations have been performed within the [1 1; −1 1] supercell expansion in order to include such antiphase displacements as well.

The vibrational modes of the Ar-MgO system can be divided into three distinct groups, which manifest very different physical character: (i) the in-slab modes, (ii) the perpendicular Ar-MgO modes, and (iii) the in-argon-monolayer modes. The vibrations of the first group are of comparatively high energy (frequencies above 160 cm^{-1}). On the other hand, these modes are quite insensitive to the presence of the argon monolayer and, hence their contribution to ΔE_{ZPE} virtually completely cancels (to a few thousandths of a kcal).

For the second type of vibrations, the displacements of the argon atoms are primarily directed perpendicular to the surface. The frequencies of such vibrations depend on the adsorption site of the vibrating argon atom and, in dense $n \times 2$ structures, on whether the displacements occur in-phase or antiphase. The latter tend to have lower frequencies, if the mutual location of some argon atoms corresponds to the repulsive side of the argon-argon potential. For example, for the sparse 2×2 structure, where the argon atoms occupy the most preferable sites only, the frequencies of the in-phase and antiphase perpendicular vibrations have virtually the same value of 34 cm^{-1}. In the other sparse 3×3 geometry with different adsorption sites being populated, the frequencies lie in the narrow window of 30–34 cm^{-1}. For the 3×2 arrangement, the in-phase vibrations have again frequencies of about 33 cm^{-1}, whereas the antiphase ones soften to 23–27 cm^{-1}. For the denser 4×2 structure, the frequencies of the antiphase vibrations drop further to 17–19 cm^{-1}.

The results for the 3×2 arrangement can be compared to those of Ref. 59, where a lattice dynamics study for this structure based on a model potential and the harmonic approximation was presented. The frequencies obtained in that work for such perpendicular modes range from 36 to 44 cm^{-1} and thus are somewhat larger than the harmonic DFT-D2 frequencies of this study. We have also calculated the frequencies of the perpendicular modes beyond the harmonic approximation by utilizing the accurate corrected LMP2 1D potentials. Within such a treatment they lie between 32 and 38 cm^{-1}, suggesting that the potential of Ref. 59 overestimates while DFT-D2 underestimates these frequencies. This anharmonic approach, however, implies independent 1D perpendicular vibrations corresponding to the in-phase modes of the sparse 2×2 structures (with which the 1D Ar-MgO potentials have been calculated, cf. Sec. II C). The frequency lowering for the antiphase modes in dense structures therefore cannot be reproduced in such a 1D treatment. In any case, despite a noticeable relative deviation in the values of the frequencies for the perpendicular vibrations within different models, their contribution $\Delta E_{\mathrm{ZPE}\perp}$ to the ZPEs is quite small, ranging from 0.03 to 0.06 kcal/mol.

The most delicate is the third group comprising the in-monolayer vibrations. The low-frequency part of these

vibrations corresponds to the movement of the argon monolayer as a whole relative to the slab in the very shallow anharmonic corrugation potential of Fig. 5. The frequencies for such vibration are very low, i.e., below 10 cm^{-1}, and depend strongly on the respective arrangement. For 3×2, one of these modes even has an imaginary frequency, which suggests a structural instability along the Mg-(Mg|Mg)-Mg direction. This coordinate leads from the periodic 3×2 to the 1D disordered $\zeta \times 2$ arrangement. The experimentally observed transition from the 3×2 phase to 4×2,[30] or the 1D melting along the Mg-(Mg|Mg)-Mg direction[28] can qualitatively be attributed to this instability, which was also noticed in the modeling of Ref. 59. Small (or imaginary) frequency values for these vibrations and the anharmonicity of the underlying potential are not harmful for the ZPE correction, since their contribution is tiny. But these modes are decisive for the finite temperature thermodynamics, which makes accurate thermodynamical modeling for this system within the harmonic approximation impossible.

The vibrations, where the argon atoms move antiphase with respect to each other, are mainly determined by the Ar-Ar interaction and thus are expected to be more energetic and less anharmonic than those discussed above. Yet this is true only for densely packed monolayers such as 3×2, hexlike, or 4×2. The frequencies of such vibrations in these arrangements can indeed reach relatively high values (e.g., up to 83 cm^{-1} in the most dense 4×2 structure) and constitute the major contribution to the overall ΔE_{ZPE}. In the sparse arrangements, on the other hand, especially those corresponding to the convex part of the lateral interaction potential, such vibrations remain very anharmonic with low frequencies. For example, for the 2×2 structure, a value of only 17 cm^{-1} is obtained, while for 3×3, some modes even have imaginary frequencies. This means that for low coverage the argon atoms on MgO do not prefer to arrange as uniform sparse structures such as 3×3, etc., but rather gather in denser islands, or form sparse $\zeta \times 2$ arrangements (e.g., 0.5×2, etc.).

As a consequence of the severe dependency of the frequencies of the in-monolayer vibrations on the density of the packing, substantial differences in the corresponding ZPE contribution $\Delta E_{\mathrm{ZPE}\,\parallel}$ for the five different arrangements studied here do occur. This is further discussed in the next section.

D. Comparison to experiment

In the previous sections, we have discussed extensively the important individual contributions to the adsorption energy at 0 K, $\Delta E_{T=0}$, which are summarized in Table II along with $\Delta E_{T=0}$ for the five arrangements studied in this work.

As anticipated, the decisive part of $\Delta E_{T=0}$ originates from the frozen core $\Delta E_{\perp}^{\mathrm{FC}}$ and $\Delta E_{\parallel}^{\mathrm{FC}}$. The other components, though correcting the value for the energy, do not alter the energetical ordering. The core-valence correlation contribution to $\Delta E_{\perp}$ is sizable, but relatively uniform among the different structures. The positive ZPEs are as important, yet not as uniform, being clearly larger for denser arrangements. At the same time, the core-valence correlation contribution to $\Delta E_{\parallel}$ as well as the surface relaxation effects turn out to be minute.

Its sparsity, and thus its weak lateral binding $\Delta E_{\parallel}$ combined with a nonoptimal Ar-MgO interaction $\Delta E_{\perp}$ renders the 3×3 structure as energetically noncompetitive. Also the sparse 2×2 arrangement, despite of featuring the largest $\Delta E_{\perp}$, is not competitive due to its too weak $\Delta E_{\parallel}$. Even though the relatively small ZPE contribution shifts the 2×2 adsorption energy towards that of the dense structures, it still remains clearly above the latter.

TABLE II. Calculated adsorption energy at 0 K, $\Delta E_{T=0}$ and its components for different arrangements of argon monolayer on the MgO(100) surface (all values in kcal/mol). The Ar-MgO and lateral frozen-core energies $\Delta E_{\perp}^{\mathrm{FC}}$ and $\Delta E_{\parallel}^{\mathrm{FC}}$ correspond to the full supercell corrected-LMP2 Ar-MgO and LMP2 Ar-monolayer calculations, respectively. The lateral and Ar-MgO core components $\Delta E_{\parallel}^{\mathrm{core}}$ and $\Delta E_{\perp}^{\mathrm{core}}$, respectively, are calculated at the periodic LMP2 level [for the latter, the sinelike representation of the potential of Eq. (3) has been used]. The effect of the surface relaxation on the binding energy $\Delta E_{\mathrm{Relax}}$ and the ZPE contributions $\Delta E_{\mathrm{ZPE}\,\perp}$ and $\Delta E_{\mathrm{ZPE}\,\parallel}$ are evaluated using the DFT-D2 method.

Structure	3×3	2×2	3×2	Hexlike	4×2
$\Delta E_{\perp}^{\mathrm{FC}}$	−1.509	−1.709	−1.601	−1.506	−1.611
$\Delta E_{\parallel}^{\mathrm{FC}}$	−0.321	−0.463	−0.707	−0.822	−0.722
$\Delta E_{\perp}^{\mathrm{core}}$	−0.147	−0.168	−0.155	−0.147	−0.155
$\Delta E_{\parallel}^{\mathrm{core}}$	−0.005	−0.009	−0.023	−0.026	−0.036
$\Delta E_{\mathrm{Relax}}$	0.024	0.031	0.027	0.027	0.022
$\Delta E_{\mathrm{ZPE}\,\perp}$	0.045	0.048	0.040	0.038	0.033
$\Delta E_{\mathrm{ZPE}\,\parallel}$	0.025	0.038	0.099	0.098	0.140
$\Delta E_{T=0}$	−1.888	−2.232	−2.320	−2.338	−2.329

The three remaining structures have very similar values for the frozen-core $\Delta E_{\perp}^{\mathrm{FC}} + \Delta E_{\parallel}^{\mathrm{FC}}$ energy and also for the total adsorption energy $\Delta E_{T=0}$ itself. As was discussed above, the 3×2 and 4×2 apparently have virtually identical lateral and perpendicular interaction energies. The hexlike structure wins in $\Delta E_{\parallel}$, but by approximately the same amount loses in $\Delta E_{\perp}$. Consequently, these three structure are expected to be nearly equally probable at $T = 0$ K, and delicate thermal or pressure effects within the actual experimental conditions decide in favor or against of one arrangements over the other. Indeed, all these three structures have been observed in experimental studies, although a conclusive picture was not yet provided by the experiments. All of them agree on the 3×2 structure appearing in moderate coverage conditions. However, for higher coverages the observed arrangement was reported to switch either to hexagonal (for $49 < T < 66$ K,[29] or for $T = 10$ K on a highly homogeneous MgO surface[28]) or to a 4×2 arrangement (for $25 < T < 36$ K).[30] In the latter case, a transition to the hexagonal structure is also observed, but only after completion of the first layer condensation. Our calculations predicting these three structures as energetically competitive are clearly in line with the experimental observations and provide an important improvement over the model potential study of Ref. 30, which rejects the hexagonal structure.

According to Table I and Fig. 7, also a large range of intermediate 1D noncommensurate $\zeta \times 2$ structures have energies close to those of 3×2 and 4×2. The intermediate structures in the $3 \times 2 \rightarrow 4 \times 2$ transition clearly manifest in the experimental data of Ref. 30, while Ref. 28 reports the 1D $n \times 2 \rightarrow \zeta \times 2$-like melting and the anomalously low triple-point temperatures associated with it. Both facts are explained

by these theoretical results. Furthermore, since the potential curves for $\zeta \times 2$ and the noncommensurate hexagonal argon monolayer virtually overlie each other at low and intermediate coverages (cf. Fig. 7), the entire loss of registry in a transition from $\zeta \times 2$ to hexagonal (which costs about 0.1 kcal/mol according to Table I) is not compensated sufficiently by the gain in the lateral interactions. The monolayer thus remains in a $\zeta \times 2$ (or $n \times 2$) arrangement at low and intermediate coverages. Figure 7 shows, that the counterbalance between the weaker Ar-MgO interactions and optimal 2D hexagonal packing occurs only for quite dense structures, i.e., at the limiting coverages of the first argon monolayer. This is exactly what has been observed in Ref. 28, where the transition $3 \times 2 \rightarrow$ hexagonal takes place at high coverage. Furthermore, since the loss of registry in the transition from $\zeta \times 2$ (or $n \times 2$) to a 2D noncommensurate structure implies a barrier of about 0.1 kcal/mol (due to the immediate increase of $\Delta E_{\perp}$ from -1.609 to -1.528 kcal/mol per Ar atom, cf. Table I) a higher temperature as in Ref. 29, or the additional interaction with second layer atoms as in Ref. 30 may be required to end up with the hexagonal arrangement.

A one-to-one comparison of the calculated $\Delta E_{T=0}$ on the one hand, and the experimentally "measured" adsorption energies at nonzero temperature on the other hand, is difficult. The calculation of vibrational frequencies is presently limited to the DFT-D2 level within the harmonic approximation. However, as discussed in Sec. III C, this is an entirely unsuitable model for the present case due to the strongly anharmonic and shallow interaction potential. Since, in contrast to the ZPE corrections, the low-frequency modes have a major influence on finite-temperature thermodynamic quantities, entropic, and enthalpic terms, evaluated within an inappropriate harmonic model, would just spoil the accuracy of the calculated $\Delta E_{T=0}$ values. Furthermore, the reported experimental energies are in fact not measured directly, but rather deduced from the measured data on the basis of certain models.

Nevertheless, assuming that (i) finite-temperature thermodynamic effects are small, and (ii) that the aforementioned models utilized to deduce the experimental energies or heats are sufficiently accurate, we now compare our $\Delta E_{T=0}$ values directly to the experimental nonzero temperature results. High-temperature ($49 < T < 66$ K) values for the isosteric heat associated with the 3D gas $\rightarrow$ 2D liquid transition,[30] are reported as 1.98 (see Ref. 27) and 2.00 kcal/mol[29]. For the isosteric heat of the transition 3D gas $\rightarrow$ 2D solid at lower temperatures ($25 < T < 34$ K), which is more closely related to $\Delta E_{T=0}$, a value of 2.3 ± 0.3 kcal/mol is provided.[30]. Finally, a value of 2.03 ± 0.33 kcal/mol for the temperature-independent activation energy for desorption, obtained by inverting the TPD spectra on the basis of the Polanyi-Wigner equation under the assumption of first-order desorption and temperature independence of the pre-exponential, is given in Ref. 32. The agreement of our $\Delta E_{T=0}$ result of 2.34 kcal/mol with these experimental values indeed is excellent.

IV. CONCLUSIONS

An accurate and unbiased first-principle method for the calculation of physisorption on insulating surfaces has been proposed. It is based on a fully periodic local MP2 treatment with corrected (scaled) intermolecular pair energies. The correction (scaling factor for the inter pairs) is based on coupled cluster CCSD(T) calculations extrapolated to the basis set limit, carried out for finite clusters mimicking the system under study. Employing this approach, the geometrical frustration of an argon monolayer adsorbed on the MgO (100) surface was studied at high accuracy in this work. Core-valence correlation contributions to the adsorption energy are also taken into account. Zero-point energies as well as geometric relaxation energies are calculated at the level of dispersion corrected DFT. The method proposed in this work is a practical way for highly accurate studies of physisorption in relatively complicated systems with large unit cells. It has certain advantages over the technique recently proposed by Tosoni and Sauer:[6] (i) instead of using periodic DFT-D2, incrementally corrected to finite cluster MP2 results [and, for important points, to small basis set CCSD(T) results], we start here already with periodic MP2, which in turn is further corrected on the basis of finite cluster CCSD(T) calculations extrapolated to the basis set limit. (ii) The correction is not incremental, but based on the appropriate scaling of the interslab-monolayer component. This scaling factor, which automatically corrects the whole LMP2 potential surface, can be obtained from finite cluster calculations on relatively small clusters, and hence in big basis sets. Such a procedure is valid as long as the LMP2 method error of the interaction within the infinite system is reproduced by the considered cluster. An incremental approach, on the other hand, requires calculations on larger clusters and individually for each point.

Our theoretical results for Ar adsorbed on MgO (100) are in a very good agreement with the available experimental data. Taking into account the relatively large experimental error bars of ± 0.3 kcal/mol and the influence of finite temperature effects, we assume that our theoretical value of $\Delta E_{T=0} = 2.32$–2.34 kcal/mol can be considered as an accurate benchmark for further theoretical or experimental studies on this system. Our study predicts the three arrangements 3×2, 4×2, and noncommensurate hexagonal (with optimal Ar-Ar distances), as well as the 1D noncommensurate $\zeta \times 2$ structures as energetically competitive. It also suggests, that at low coverages the adsorption process starts within the $\zeta \times 2$ (and $n \times 2$) orientation. These findings are in line with the experimental observations, and also shed light on some peculiarities and controversies among the different experiments.

Finally, we note that simplified models for the Ar-MgO potential based on pairlike interactions or a sinelike representation turn out to be rather accurate. These can further be used for working out inexpensive models for extensive molecular dynamics or Monte Carlo simulations on the Ar-MgO system.

ACKNOWLEDGMENT

D.U. gratefully acknowledges the financial support from the Deutsche Forschungsgemeinschaft (Grant No. US 103/1-1).

APPENDIX A: COMPUTATIONAL PARAMETER SPECIFICATIONS

The HF and DFT-D2[40] calculations were performed using the CRYSTAL code.[34] The Mg and oxygen basis sets were taken

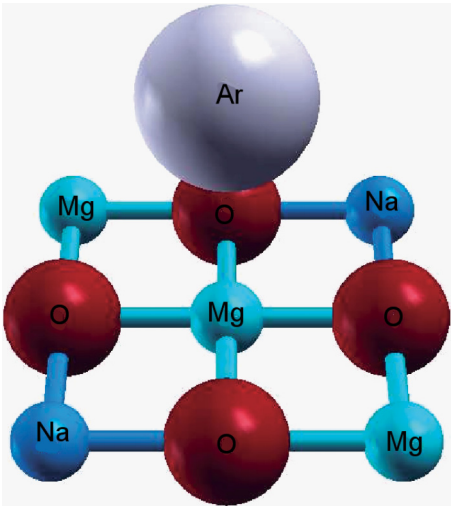

FIG. 8. (Color online) Ar-$Na_2Mg_3O_4$ dimer used in the LMP2→CCSD(T) correction scheme.

TABLE III. The x and y coordinates of the different adsorption sites (with respect to the coordinate system of Fig. 5), studied within the 2×2 supercell; the z coordinate of the minima of the 2×2 corrected-LMP2 potential curves ($R_z^{\min}$) and the corrected-LMP2 energies $\Delta E_{\perp}^{\min}$, corresponding to these minima. The values for x and y are given in the fractional units, with respect to the lattice parameter of the MgO surface $a = 2.9769$ Å.

Adsorption Position	x/a	y/a	$R_z^{\min}$, Å	$\Delta E_{\text{perp}}^{\min}$, kcal/mol
1 (on Mg)	0.5	0.5	3.29	−1.7091
2 (on oxygen)	0.0	0.0	3.55	−1.3810
3 (on Mg|Mg)	0.0	0.5	3.44	−1.5112
4	0.25	0.5	3.36	−1.6039
5	0.1667	0.5	3.40	−1.5539
6	0.0	0.25	3.50	−1.4437
7	0.0714	0.6429	3.46	−1.4821
8	0.6429	0.7857	3.41	−1.5505
9	0.2143	0.9285	3.52	−1.4301
10	0.9286	0.8571	3.54	−1.4113
11	0.3571	0.7143	3.38	−1.5873
12	0.7857	0.5714	3.39	−1.5720

from Ref. 25 (BS4: $[5s4p2d1f]$ for Mg and $[5s4p3d2f]$ for O). For the argon atoms the relativistic effective core pseudopotential and the corresponding basis set of Ref. 60, augmented with an additional f shell with exponent 0.28 a.u., i.e., $[\text{ECP};4s4p3d2f]$, was used.

In the HF (and DFT) calculations substantially tightened thresholds (relative to their defaults) of 7 7 7 25 75 were chosen for the two-electron integral prescreening (TOLINTEG parameters).[34] Different k-point meshes were chosen for different structures, depending on the related unit cell sizes: 8×8 for the 2×2 arrangement, the $\zeta \times 2$, and the hexagonal structures in the argon-monolayer only calculations; 6×6 for the 4×2-arrangement; 4×4 for the 3×2, 3×3, and hexlike arrangements. To improve the HF convergence the previous-iteration Fock-matrix mixing (FMIXING[34]) of 40% and level shifting (LEVSHIFT[34]) of 1 Hartree with the state lock were utilized. The WF[35] and PAO[33] generation employed the same k meshes as the HF calculations, apart from the case of the hexlike system, where the 2×2 k mesh was used to construct the PAOs. Furthermore, in the latter case, due to technical reasons, HF, localization and MP2 calculations were performed without including the actual (C_2) point-group symmetry.

The following orbital excitation domains[16,61] were chosen for the LMP2 calculations: one-atom domains for the Ar-centered and Mg-centered (core) WFs; for the oxygen atom WFs the domains consisted of one oxygen atom and the first coordination sphere of Mg atoms, i.e., six- and seven-atom domains for the surface and bulk oxygen WFs, respectively. The WF-pair approximations were defined on the basis of the distance between the centers of the corresponding WFs. In the calculations of $\Delta E_{\perp}$ intra-MgO or intra-Argon-monolayer pairs with inter-WF distances up to 6 Å were considered. For the inter slab-adsorbate pairs as well as for the pairs in the argon-monolayer calculations of $\Delta E_{\parallel}$ the inter-WF cutoff distance was set to 12 Å. Furthermore, the energy contributions from such pairs beyond 12 Å were added a posteriori, by assuming the $C_6 R^{-6}$ decay law and fitting the WF-pair-specific C_6 coefficients to the decay of the explicitly calculated pair energies in the range from 8 to 12 Å.[16,17]

TABLE IV. The Ar-MgO corrected LMP2 energies $\Delta E_{\perp}$ (in kcal/mol) as functions of argon-slab distance R_z, explicitly calculated for different adsorption positions within the 2×2 supercell (as defined in Table III).

	Adsorption position											
$R_z^{\min}$, Å	1	2	3	4	5	6	7	8	9	10	11	12
3.0	−1.4186	0.0286	−0.8332	−1.1533	−0.9901							
3.2	−1.6876	−0.9556	−1.3567	−1.5345	−1.4438	−1.1615	−1.3008	−1.4321	−1.1256	−1.0498	−1.5061	−1.4847
3.4	−1.6831	−1.3279	−1.5087	−1.6006	−1.5538	−1.4195	−1.4748	−1.5501	−1.3976	−1.3626	−1.5865	−1.5717
3.6	−1.5586	−1.3775	−1.4668	−1.5146	−1.4914	−1.4265	−1.4473	−1.4901	−1.4156	−1.4055	−1.5089	−1.4985
3.8	−1.3874	−1.3144	−1.3445	−1.3642	−1.3503	−1.3304	−1.3282	−1.3525	−1.3102	−1.3234	−1.3644	−1.3561
4.0	−1.2096	−1.1756	−1.1881	−1.1955	−1.1908	−1.1844	−1.1682	−1.1943	−1.1775	−1.1865	−1.1973	−1.1915
4.5	−0.8273	−0.8382	−0.8257	−0.8222	−0.8205							
5.0	−0.5646	−0.5809	−0.5688	−0.5656	−0.5624							
6.0	−0.2949	−0.3023	−0.2982	−0.2931	−0.2925							

TABLE V. Specification of the supercell geometries for the studied structures. The supercell expansions are given with respect to the two-atom MgO surface unit cell. The data refer to the primitive cells. The symbols "1×" and "2×" denote the number of symmetry equivalent adsorption sites of a certain type (as defined in Table III), which are occupied with argon atoms in each arrangement.

Structure	Supercell expansion	2D space group	N. of atoms per cell	N. of argons per cell	Adsorption positions 1×	Adsorption positions 2×
2 × 2 [see Fig. 4(a)]	(1 −1); (1 1)	$P4mm$	13	1	1	
3 × 2 [see Fig. 4(b)]	(3 0); (0 2)	$Pmm2$	40	4	1, 3	4
4 × 2 [see Fig. 4(c)]	(2 1); (−2 1)	$Cmm2$	27	3	1	5
3 × 3 [see Fig. 4(d)]	(3 0); (0 3)	$Pmm2$	58	4	1, 3	6
Hexlike [see Fig. 4(e)]	(2 −1); (4 8)	$P211$	134	14	1, 3	7–12

The same C_6 coefficients were used to approximate the dispersion contribution to $\Delta E_\perp$ from a semi-infinite MgO solid, using the slab replication technique.[17] The direct-space local robust density fitting technique[22] was employed for the two-electron integrals with interorbital distance up to 8 Å. Beyond this distance, the integrals were evaluated by means of the multipolar approximation. For density fitting, a combined Poisson-GTO-type fitting basis set[22,62,63] was used, which was converted[22] from the pure GTO auxiliary basis set optimized for the MP2 aug-cc-pVTZ calculations.[64] The redundancy parameter for the pair-domain-specific PAOs[16] was set to 10^{-5}.

For the geometry relaxation and frequency calculations, carried out at the DFT-D2 (PBE) level, a reduced basis was employed: the most diffuse d and f functions (on oxygen both f functions) were omitted. The D parameters for Argon were taken from Ref. 40, while those for Mg and O from Ref. 6. Dense grids: XXLGRID[34] were used for the numerical evaluation of the PBE exchange-correlation integrals. In the frequency calculations of the hexlike structure only a submatrix of the Hessian, related to the modes of the argon atoms, was computed.

APPENDIX B: SPECIFICATION OF THE LMP2→CCSD(T) CORRECTION SCHEME

The correcting factor f_{inter} for scaling the inter-adsorbate-slab correlation energy was evaluated by finite cluster calculations, carried out with the MOLPRO program.[65,66] As the prototype system the dimer shown in Fig. 8, closely related to the periodic problem under study, was employed. It consists of a square cluster $Na_2Mg_3O_4$ with the same oxygen-metal distance as in the MgO slab (2.105 Å) and an argon atom, positioned on top of the central Mg atom. The counterpoise-corrected interaction energies for different Ar-Mg distances R_z (2.75 Å bis 8 Å) were calculated (i) at the CCSD(T) level with the aug-cc-pVTZ and aug-cc-pVQZ basis sets, and subsequent inverse-cubic extrapolation of the correlation energy; and (ii) with the local MP2 method in the same AVTZ' basis as used in the periodic calculations. Furthermore, in order to enhance the similarity between the periodic and cluster LMP2 calculations, the computational parameters of the latter were chosen to be as close to the former as possible. That is, (i) the Mg-AVTZ' basis set was used for the Na atoms, as well; (ii) one-atom domains were employed for Ar-WFs, and six-atom ones for the oxygen WFs: each oxygen atom was surrounded by additional ghost Mg-atoms; (iii) the localized orbitals were constructed via the Boys localization procedure;[67] and (iv) the value of 10^{-5} was used for the pair-domain-specific PAO redundancy threshold. The correlation part of the LMP2 interaction energy was partitioned[47] into intra-$Na_2Mg_3O_4$ energy $\Delta E^{\text{LMP2}}_{\text{intra-cl.}}$, intra-argon energy $\Delta E^{\text{LMP2}}_{\text{intra-Ar}}$ and intermonomer $\Delta E^{\text{LMP2}}_{\text{inter}}$ energy. The scaling factor f_{inter} was obtained by minimizing $\sum_{\{R_z\}}(\Delta E^{\text{CCSD(T)}} - \Delta E^{\text{LMP2}}_{\text{intra-cl.}} - \Delta E^{\text{LMP2}}_{\text{intra-Ar}} - f_{\text{inter}}\Delta E^{\text{LMP2}}_{\text{inter}})^2$, where $\Delta E^{\text{CCSD(T)}}$ stands for the correlation contribution to the binding energy at the CCSD(T) level.

APPENDIX C: THE INDIVIDUAL 2 × 2 GEOMETRIES FOR DIFFERENT ADSORPTION POSITIONS AND CORRESPONDING $\Delta E_\perp$ ENERGIES

In the following, the geometries of the studied systems and obtained interaction energies $\Delta E_\perp$ are given. Table III provides the x and y coordinates of the 12 adsorption sites, for which the individual potential energy curves $\Delta E_\perp(R_z)$ were calculated within the 2 × 2 supercell. The R_z coordinates for the minima of these curves as well as the corresponding energy values are given in the same table. The full curves calculated for $3.2 \leqslant R_z \leqslant 4.0$ Å, and for some adsorption sites for $3.0 \leqslant R_z \leqslant 6.0$, are compiled in Table IV. These data can be used to approximate the 3D argon-MgO potential energy surface within this range of the R_z distances. Finally, the detailed geometry specifications of the five studied arrangements of frustrated argon monolayers, adsorbed on the MgO (100) surface are presented in Table V.

*denis.usvyat@chemie.uni-regensburg.de
†martin.schuetz@chemie.uni-regensburg.de

[1] R. Ahlrichs, R. Penco, and G. Scoles, Chem. Phys. **19**, 119 (1979).
[2] M. Elstner, P. Hobza, T. Frauenheim, S. Suhai, and E. Kaxiras, J. Chem. Phys. **114**, 5149 (2001).
[3] Q. Wu and W. Yang, J. Chem. Phys. **116**, 515 (2002).
[4] U. Zimmerli, M. Parrinello, and P. Koumoutsakos, J. Chem. Phys. **120**, 2693 (2004).
[5] S. Grimme, J. Comp. Chem. **25**, 1463 (2004).
[6] S. Tosoni and J. Sauer, PhysChemChemPhys **12**, 14330 (2010).

[7] J. Harl and G. Kresse, Phys. Rev. Lett. **103**, 056401 (2009).
[8] J. Paier, B. G. Janesko, T. M. Henderson, G. E. Scuseria, A. Grüneis, and G. Kresse, J. Chem. Phys. **132**, 094103 (2010).
[9] G. E. Scuseria, T. M. Henderson, and D. C. Sorensen, J. Chem. Phys. **129**, 231101 (2008).
[10] I. Schmitt, K. Fink, and V. Staemmler, PCCP **11**, 11196 (2009).
[11] C. Müller, B. Herschend, K. Hermansson, and B. Paulus, J. Chem. Phys. **128**, 214701 (2008).
[12] E. Voloshina, D. Usvyat, M. Schütz, Y. Dedkov, and B. Paulus, PhysChemChemPhys **13**, 12041 (2011).
[13] C. Müller and K. Hermansson, Surf. Sci. **603**, 3329 (2009).
[14] C. Müller, D. Usvyat, and H. Stoll, Phys. Rev. B **83**, 245136 (2011).
[15] C. Müller and D. Usvyat, *Incremental corrections to the periodic local MP2 method* (unpublished).
[16] C. Pisani, L. Maschio, S. Casassa, M. Halo, M. Schütz, and D. Usvyat, J. Comp. Chem. **29**, 2113 (2008).
[17] C. Pisani, M. Schütz, S. Casassa, D. Usvyat, L. Maschio, M. Lorenz, and A. Erba, PCCP **14**, 7615 (2012).
[18] A. Grüneis, M. Marsman, and G. Kresse, J. Chem. Phys. **133**, 074107 (2010).
[19] S. Saebø and P. Pulay, Chem. Phys. Lett. **113**, 13 (1985).
[20] M. Schütz, G. Hetzer, and H. J. Werner, J. Chem. Phys. **111**, 5691 (1999).
[21] L. Maschio and D. Usvyat, Phys. Rev. B **78**, 073102 (2008).
[22] M. Schütz, D. Usvyat, M. Lorenz, C. Pisani, L. Maschio, S. Casassa, and M. Halo, in *Accurate Condensed Phase Quantum Chemistry*, edited by F. R. Manby (CRC, Boca Raton, FL, 2010), p. 29.
[23] L. Maschio, D. Usvyat, M. Schütz, and B. Civalleri, J. Chem. Phys. **132**, 134706 (2010).
[24] L. Maschio, D. Usvyat, and B. Civalleri, Cryst. Eng. Comm. **12**, 2429 (2010).
[25] R. Martinez-Casado, G. Mallia, D. Usvyat, L. Maschio, S. Casassa, M. Schütz, and N. Harrison, J. Chem. Phys. **134**, 014706 (2011).
[26] R. Martinez-Casado, G. Mallia, D. Usvyat, L. Maschio, S. Casassa, M. Schütz, and N. M. Harrison, PhysChemChemPhys **13**, 14750 (2011).
[27] J.-P. Coulomb, T. S. Sullivan, and O. E. Vilches, Phys. Rev. B **30**, 4753 (1984).
[28] J.-P. Coulomb, in *Phase transitions in Surface Films 2*, edited by H. Taub, G. Torzo, H.-J. Lauter, and S. C. Fain (Plenum, New York, 1991), p. 113.
[29] K. Madih, Ph.D. thesis, Universite d'Aix-Marseille II, 1986.
[30] T. Meichel, J. Suzanne, C. Girard, and C. Girardet, Phys. Rev. B **38**, 3781 (1988).
[31] J. M. Layet, M. Bienfait, C. Ramseyer, P. N. M. Hoang, C. Girardet, and G. Coddens, Phys. Rev. B **48**, 9045 (1993).
[32] Z. Dohnalek, R. S. Smith, and B. D. Kay, J. Phys. Chem. B **106**, 8360 (2002).
[33] D. Usvyat, L. Maschio, C. Pisani, and M. Schütz, Z. Phys. Chem. **224**, 441 (2010).
[34] R. Dovesi *et al.*, CRYSTOL09 *User's Manual*, Università di Torino, Torino (2010), http://www.crystal.unito.it.
[35] C. M. Zicovich-Wilson, R. Dovesi, and V. R. Saunders, J. Chem. Phys. **115**, 9708 (2001).
[36] S. Casassa, C. M. Zicovich-Wilson, and C. Pisani, Theor. Chem. Acc. **116**, 726 (2006).
[37] S. Boys and F. Bernardi, Mol. Phys. **19**, 553 (1970).
[38] K. A. Peterson and T. H. Dunning, J. Chem. Phys. **117**, 10548 (2002).
[39] J. P. Perdew, K. Burke, and M. Ernzerhof, Phys. Rev. Lett. **77**, 3865 (1996).
[40] S. Grimme, J. Comp. Chem. **27**, 1787 (2006).
[41] B. Civalleri, C. M. Zicovich-Wilson, L. Valenzano, and P. Ugliengo, Cryst. Eng. Comm. **10**, 405 (2008).
[42] K. Doll, V. Saunders, and N. Harrison, Int. J. Quantum. Chem. **82**, 1 (2001).
[43] F. Pascale, C. M. Zicovich-Wilson, F. L. Gejo, B. Civalleri, R. Orlando, and R. Dovesi, J. Comp. Chem. **258**, 888 (2003).
[44] P. Ugliengo, ANHARM: *A Program to Solve Monodimensional Nuclear Schrödinger Equation* (1989) (unpublished).
[45] D. Usvyat, B. Civalleri, L. Maschio, R. Dovesi, C. Pisani, and M. Schütz, J. Chem. Phys. **134**, 214105 (2011).
[46] S. J. Nolan, M. J. Gillan, D. Alfè, N. L. Allan, and F. R. Manby, Phys. Rev. B **80**, 165109 (2009).
[47] M. Schütz, G. Rauhut, and H.-J. Werner, J. Phys. Chem. A **102**, 5997 (1998).
[48] H.-J. Werner and M. Schütz, J. Chem. Phys. **135**, 144116 (2011).
[49] J. Yang, G. K.-L. Chan, F. R. Manby, M. Schütz, and H.-J. Werner, J. Chem. Phys. **136**, 144105 (2011).
[50] T. Helgaker, P. Jørgensen, and J. Olsen, *Molecular Electronic Structure Theory* (John, Chichester, UK, 2000).
[51] R. A. Kendall, T. H. Dunning, and R. J. Harrison, J. Chem. Phys. **96**, 6796 (1992).
[52] A. Heßelmann, J. Chem. Phys. **128**, 144112 (2008).
[53] A. Grüneis, G. H. Booth, M. Marsman, J. Spencer, A. Alavi, and G. Kresse, J. Chem. Theory Comput. **7**, 2780 (2011).
[54] D. Usvyat, *Van der Waals dispersion in the local correlation energy partitioning* (unpublished).
[55] J. Langlet, J. Caillet, J. Bergès, and P. Reinhardt, J. Chem. Phys. **118**, 6157 (2003).
[56] S. Grimme, J. Chem. Phys. **118**, 9095 (2003).
[57] S. Grimme, J. Chem. Phys. **124**, 034108 (2006).
[58] A. Tkatchenko, R. A. DiStasio, M. Head-Gordon, and M. Scheffler, J. Comp. Phys. **131**, 094106 (2009).
[59] C. Girardet and C. Girard, Phys. Rev. B **39**, 8643 (1989).
[60] A. Nicklass, M. Dolg, H. Stoll, and H. Preuss, J. Chem. Phys. **102**, 8942 (1995).
[61] A. Erba and M. Halo, CRYSCOR09 *User's Manual*, Università di Torino, Torino (2010), http://www.cryscor.unito.it.
[62] F. R. Manby, P. J. Knowles, and A. W. Lloyd, J. Chem. Phys. **115**, 9144 (2001).
[63] J. W. Mintmire and B. I. Dunlap, Phys. Rev. A **25**, 88 (1982).
[64] F. Weigend and R. Ahlrichs, PhysChemChemPhys **7**, 3297 (2005).
[65] H.-J. Werner, P. J. Knowles, G. Knizia, F. R. Manby, and M. Schütz, Comput. Mol. Sci. **2**, 242 (2011).
[66] H.-J. Werner *et al.*, MOLPRO, *Version 2008.2, a Package of Ab Initio Programs* (2009), see http://www.molpro.net.
[67] S. F. Boys, in *Quantum Theory of Atoms, Molecules, and the Solid State*, edited by P. O. Löwdin (Academic Press, New York, 1966), pp. 253–262.